Origin of the extreme and anisotropic magnetoresistance in the Weyl semimetal NbP

F. Balduini,[1,*] A. Molinari,[1] L. Rocchino,[1] V. Hasse,[2] C. Felser,[2] C. Zota,[1] H. Schmid,[1] and B. Gotsmann[1,†]
[1]*IBM Research Europe - Zurich, 8803 Ruschlikon, Switzerland*
[2]*Max Planck Institute for Chemical Physics of Solids, 01187 Dresden, Germany*

(Received 3 April 2023; accepted 9 January 2024; published 29 January 2024)

The fascination with semimetals, especially Dirac and Weyl semimetals, is given by their surprisingly strong response to magnetic fields. In particular, the extremely large magnetoresistance (XMR), i.e., the change in electrical resistivity as a function of the applied magnetic field, has attracted interest because of its deviation by several orders of magnitude from the behavior of normal metals, and its potential for technological applications. To date, it is unclear if the XMR in topological semimetals is inherently correlated to the very high electron mobility and electron-hole compensation, or to other exotic mechanisms. Here, we show that the relativistic and topological nature of charge carriers of the Weyl semimetal niobium phosphide (NbP) are only indirect causes of the XMR. Instead, the XMR can be explained by the very long mean free path $l_e(4\ \mathrm{K}) \approx 8\ \mu\mathrm{m}$ in combination with the small cyclotron orbits emerging in the presence of a magnetic field $r_c(9\ \mathrm{T}) \approx 20$ nm of the NbP's Weyl electrons. More precisely we find $\mathrm{MR} = c\, l_e/r_c$, where c is a parameter independent of temperature and angle between the magnetic field and the crystal. To demonstrate, we use temperature and angle-dependent magnetoresistance measurements, and extract the mean free path and cyclotron radius from an analysis of the Shubnikov–de Haas oscillation.

DOI: 10.1103/PhysRevB.109.045148

I. INTRODUCTION

Since the discovery of topological semimetals, one of the properties that drew particular attention is their extremely large magnetoresistance (XMR), which can achieve values up to a few million percent at low temperatures and high magnetic fields (WP_2: 4×10^6% [1], NbP: 8.5×10^5% [2], CdAs: 1.3×10^6% [3], TaP: 1.8×10^6% [4], at 2 K and 9 T). These values are astonishing when compared to the few percent change in resistance of conventional metals in a high magnetic field. In addition, XMR also exceeds typical values of giant magnetoresistance [5] or colossal magnetoresistance [6], making XMR materials appealing for technological applications [7].

The substantial deviation from normal metals suggests that the XMR in topological semimetals originates from unusual mechanisms [8–10], none of which has been conclusively confirmed. Electron-hole compensation and ultrahigh carrier mobility are common characteristics of semimetals, and their combination is arguably the most popular explanation for the XMR [8,11–16]. In fact, classically, the coexistence of multiple pockets with similar electron and hole carrier densities is needed to explain the nonsaturating and nonparabolic MR typical of semimetals. Only a perfect compensation brings $\mathrm{MR} = \frac{\rho(B)-\rho(0)}{\rho(0)} \sim B^2$, where ρ is the electrical resistivity and B is the magnetic field [17,18], and the closer the system is to compensation and the higher the mobility of the carriers, the larger is the MR.

The dependence of the MR on mobility is more rigorously captured by Kohler's rule, which states that the MR of a metal is solely a function of the ratio B/ρ_0, where ρ_0 is the resistivity at $B = 0$ [19]. The rationale is based on simple scaling arguments to consider a shortening of the mean free scattering distance through the application of a magnetic field, which says that the MR is determined by l_e/r_c, where l_e is the mean free path of charge carriers and r_c the cyclotron radius [17,20]. But since $l_e \propto \rho_0^{-1}$ and $r_c \propto B^{-1}$, the MR can be considered to depend only on the ratio B/ρ_0. The validity of Kohler's rule $\mathrm{MR} = f(B/\rho_0)$ has been demonstrated for XMR materials with a relatively large Fermi energy, such as WTe_2 [16].

However, when the Fermi energy is small, the mean free path $l_e = \frac{\hbar k_F}{e}\mu = \frac{\hbar k_F}{ne^2\rho_0}$, where k_F is the Fermi momentum, e the elemental charge, and μ the charge mobility, depends on the temperature by both $\rho_0(T)$ and the temperature-dependent carrier density $n(T)$. Therefore, an extended Kohler's rule must be used, according to which the temperature dependence of l_e is linked to the temperature-dependent mobility μ, rather than just ρ_0, implying $\mathrm{MR} = f(B\mu)$ [21]. This has been demonstrated for the XMR Weyl semimetal TaP using density functional theory (DFT) calculations to extract the carrier density [22].

In order to investigate the origin of the XMR in Weyl semimetals, here we test the validity of the more general $\mathrm{MR} = f(l_e/r_c)$ for NbP, relying exclusively on Shubnikov–de Haas (SdH) oscillations to estimate l_e and r_c, and taking advantage of the anisotropic Fermi surface (FS) of NbP to go beyond the approximation $r_c \propto B^{-1}$. In particular, we show that (a) the temperature dependence of the MR correlates to the temperature dependence of the mean free path l_e, or mobility μ; and (b) the angle-dependent MR correlates to the

*ico@zurich.ibm.com
†bgo@zurich.ibm.com

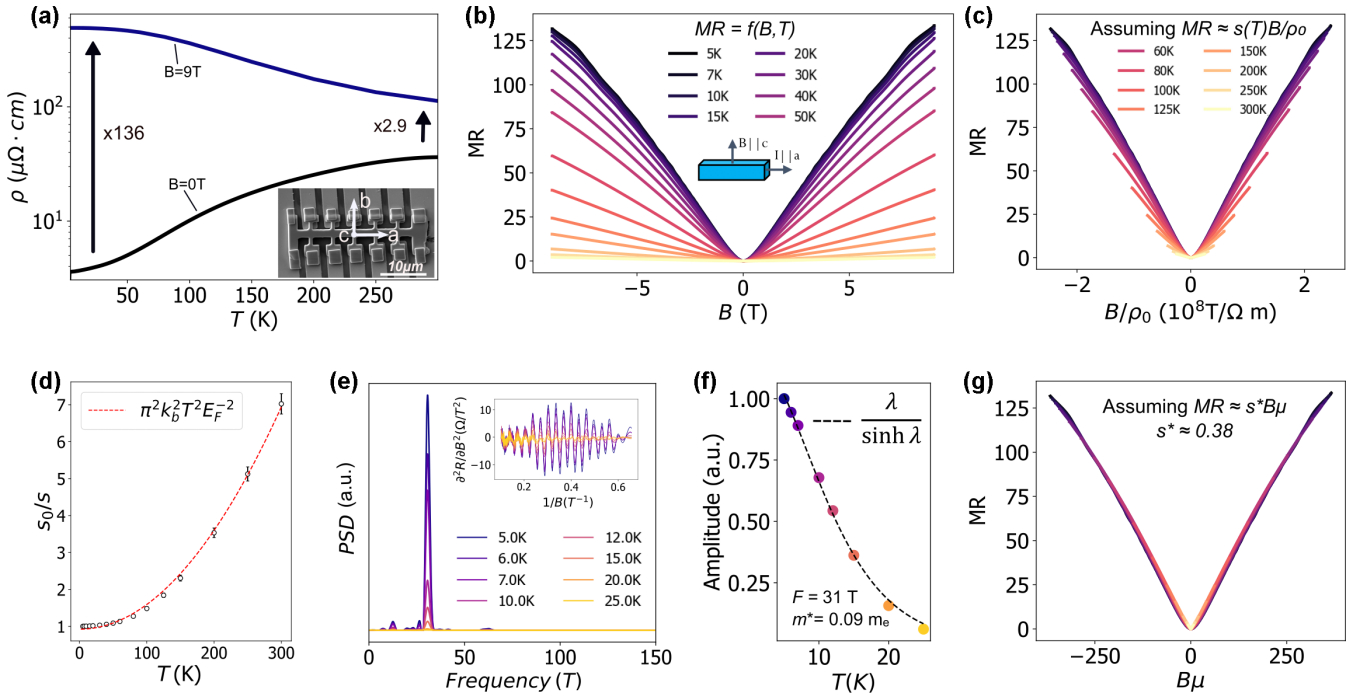

FIG. 1. Magnetoresistance and mobility. (a) Resistivity vs temperature of the NbP Hall bar shown in the inset, for $B = 0$ T (black) and $B = 9$ T (blue). (b) MR as a function of field B, for $B \parallel c$ at various temperatures. (c) When plotted against B/ρ_0 the MR curves at various temperatures do not collapse on a single line, i.e., the angular coefficient s in MR $= sB/\rho_0$ is temperature dependent. (d) The temperature dependence of s is well described by a parabolic function. Assuming that this is due to the temperature-dependent carrier density, the experimental points are fitted according to Eq. (1) to extract the Fermi energy $E_F^s \approx 33$ meV. (e) Frequency spectrum of the SdH oscillations, shown in the inset. (f) Temperature dependence of the SdH oscillation amplitude. The dotted line shows the Lifshitz-Kosevich fit from which the effective mass is extracted, which, combined with the oscillations' frequency, is used to estimate the Fermi energy $E_F^{\mathrm{SdH}} \approx 37$ meV, which in turn is used to calculate the mobility μ. (g) MR as a function of field times mobility at various temperatures. The MR curves collapse on a single line, showing that its temperature dependence comes from temperature-dependent mobility.

length of the cyclotron radius r_c, which is a function of the cross-sectional FS area perpendicular to B. In other words, we propose that not only the high mobility but, independently, also the small FS of NbP are responsible for the XMR.

Importantly, despite the complicated FS of NbP and the presence of many carrier pockets (i.e., a multitude of small FSs) [23], the temperature and angle dependence of the MR can be understood by considering only the carriers which dominate quantum oscillations, ignoring trivial pockets with larger effective mass.

II. EXPERIMENT

High-quality single bulk crystals of NbP were grown via a chemical vapor transport reaction using an iodine transport agent. A polycrystalline powder of NbP was synthesized by a direct reaction of niobium (Chempur 99.9%) and red phosphorus (Heraeus 99.999%) within an evacuated fused silica tube for 48 h at 800 °C. The growth of bulk single crystals of NbP was then initialized from this powder by chemical vapor transport in a temperature gradient, starting from 850 °C (source) to 950 °C (sink) and a transport agent with a concentration of 13.5 mg cm^{-3} iodine (Alfa Aesar 99.998%).

Microscopic bars were extracted from a single crystal by means of focused ion beam (FIB) microstructuring [24], which allows for high aspect-ratio samples with good control of geometry and crystalline direction, and homogeneous magnetic field distribution along the sample. As a drawback, the properties of a thin superficial layer are altered [25], nevertheless, bulk properties are unchanged as demonstrated by the good match between quantum oscillations in microstructured and bulk samples. After the milling procedure, the sample was placed on a prepatterned chip and contacted by ion-assisted chemical vapor deposition of platinum (contact resistance around 15 Ω).

Electrical measurements were performed in a cryostat (Dynacool from Quantum Design) using external lock-in amplifiers (MFLI from Zurich Instruments). The electrical current was always applied along the same crystalline direction, and for the angle-dependent measurements, the magnetic field was rotated keeping a 90° orientation with respect to the current. The results were confirmed on a second sample (see Supplemental Material [26]).

III. RESULTS AND DISCUSSION

A. Magnetoresistance and mobility

Figures 1(a) and 1(b) show the temperature-dependent MR of the NbP Hall bar. It has a resistivity of 38.3 μΩ cm at 300 K and 3.6 μΩ cm at 4.2 K (RRR ∼ 11). The MR at 9 T for a magnetic field parallel to the c axis increases from 295% at 300 K to 13.600% at 4.2 K. At sufficiently high magnetic fields the temperature coefficient of the resistivity becomes negative (insulatinglike behavior [10,16]).

Figure 1(b) shows the MR of NbP at various temperatures T, for B parallel to the c axis, and perpendicular to the electrical current. The MR does not saturate and exhibits a parabolic to nearly linear transition at a critical field of around 0.5 T (as visible from the derivative of the MR in the Supplemental Material [26]). The nonsaturating and approximately linear MR is widely observed in semimetals [3,10,27–29], but unexpected from the classical theory of MR based on Lorentz force, indicating that some more complex mechanisms come into play. Nevertheless, the application of Kohler's rule can offer insights into the factor that regulates the magnitude of the MR.

The MR is approximately linear in the range under analysis (0–9 T, 4–300 K), so according to Kohler's rule, it should be a temperature-independent linear function of B/ρ_0. This is only approximately the case, as shown in the so-called Kohler plot in Fig. 1(c).

To improve the Kohler scaling, we need to move to an extended Kohler's rule by considering the temperature dependence of the carrier density. We can rely exclusively on the MR data and extract E_F from the SdH oscillations emerging at low temperatures, and find the temperature dependence of the carrier density n at E_F from the Sommerfeld expansion,

$$n(T) = \int_0^\infty f(\epsilon)g(\epsilon)d\epsilon \approx \frac{E_F^3}{3\pi^2(\hbar v_F)^3}\left(1+\pi^2 k_b^2 T^2 E_F^{-2}\right), \tag{1}$$

where $f(\epsilon) = \frac{1}{1+e^{(\epsilon-E_F)/k_BT}}$ is the Fermi-Dirac distribution, $g(\epsilon) = \frac{\epsilon^2}{\pi^2(\hbar v_F)^3}$ is the density of states (DOS) for relativistic carriers, and v_F is the Fermi velocity.

The carrier density goes approximately as $n \sim T^2$, which is also the trend followed by the inverse of the angular coefficients $s(T)^{-1}$ extracted from a linear fit of MR $= s(T)B/\rho_0$, as shown in Fig. 1(d). Assuming that the MR depends on temperature only through $\rho_0(T)$ and $n(T)$, then $s(T)^{-1} \propto n(T)$, and, according to Eq. (1), a parabolic fit of $\frac{s(0)}{s(T)} = \frac{n(T)}{n(0)}$ would return the Fermi level as the only free parameter. From the fit, we find $E_F = 33$ meV. Now, we will compare this value with the one extracted from the SdH oscillations.

After isolating the SdH oscillations from a smooth background by computing the second derivative of the MR [inset in Fig. 1(e)], we extract the power spectral density (PSD), shown in Fig. 1(e), to calculate the cross-sectional Fermi-surface areas according to the Onsager relation $A_{FS} = (2\pi^2/\Phi_0)F$, where $\Phi_0 = 2.07 \times 10^{-15}$ T m^2 is the flux quantum, and F is the oscillation frequency. We find a dominant PSD at 31 T. Then, we find the effective mass m^* of the carriers related to such a frequency by fitting the temperature dependence of the amplitude A of the 31-T peak in the PSD, using the Lifshitz-Kosevich formula $A = \frac{\lambda}{\sinh(\lambda)}$, where $\lambda = 14.7\frac{T}{Bm^*}$ [Fig. 1(f)]. Finally, the Fermi energy is calculated as $E_F = \frac{\hbar^2 k_F^2}{2m^*}$, where $k_F = \sqrt{A_{FS}/\pi}$ is the Fermi momentum, assuming a circular cross-sectional FS. We find $E_F = 37$ meV, comparable with the value found from the fit in Fig. 1(d). Given E_F, the carrier density is calculated from Eq. (1) (considering the anisotropy of the FS, according to the data discussed below), and the mobility as $\mu = (ne\rho_0)^{-1}$. Now, when we plot the MR as a function of $B\mu$, we get the collapse expected for the Kohler's plot [Fig. 1(g)], indicating that the temperature dependence of the MR comes from the temperature-dependent mobility, or mean free path l_e, of the carriers that dominate the SdH's PSD. A similar analysis has also been done by Xu *et al.*, however, in Ref. [22] the authors had to rely on DFT calculations to predict the carrier density, while here we show that it can be found from experiments alone.

The mobility turns out to be extremely large, especially at low temperatures: $\mu(5\text{ K}) = 4 \times 10^5$ cm^2/V s and $\mu(300\text{ K}) = 7 \times 10^3$ cm^2/V s, and this is the first out of two causes for the XMR in the Weyl semimetal NbP. In this sense, the relativistic nature of the carriers in NbP plays a major role, first of all, because of their intrinsically small effective mass $m^* = 0.09m_e$, which directly influences the mobility ($\mu = \frac{e\tau}{m^*}$, where τ is the carrier scattering time); second, the relativistic DOS causes a steeper increase of the carrier density as the temperature increases, which is partially responsible for the strong decrease of the mobility, and therefore of the MR, at high temperatures.

B. Angle-dependent magnetoresistance and Fermi-surface anisotropy

After having verified that the XMR is a linear function of the mean free path, we investigate whether the magnetoresistance of NbP increases linearly as the cyclotron radius decreases, as expected if MR $\propto \frac{l_e}{r_c}$. To do so, we take advantage of the anisotropic Fermi surface of NbP [23]. The anisotropicity of the FS reflects in the change of the carriers' cyclotron orbit as the magnetic field is rotated with respect to the crystalline axes. In fact, the cyclotron orbit is equal to the FS contour perpendicular to B and scaled by $\hbar/eB$. Figure 2(a) shows that the MR of NbP manifests a similar anisotropic character, namely, it changes as the magnetic field is rotated. Next, we will show that the change of the cyclotron orbit dimension can quantitatively account for the measured anisotropic MR.

By means of angle-dependent SdH measurements [Fig. 2(b)] we reconstruct the evolution of the cross-sectional FS area as a function of the angle ϕ between B and the c axis of the NbP crystal. The FS area is proportional to the SdH oscillation frequency, and the number of mixing frequencies reflects the number of carrier pockets populating NbP. Three peaks are distinguishable in the PSD in Fig. 2(c), and are characterized by a similar trend: The oscillation frequency, and so FS's area perpendicular to B, increase as the magnetic field is rotated from being parallel to the c axis to being parallel to the b axis. The simplest FS shape with such characteristics is an ellipsoid sphere, in which case the angular-dependent SdH frequency is $F(\phi) = F(0^\circ)F(90^\circ)\sqrt{\frac{\cot^2\phi+1}{F(90^\circ)^2\cot^2\phi+F(0^\circ)^2}}$ [30]. This relation, plotted in dashed lines in Fig. 2(d), describes the experimental data reasonably well.

As the cross-sectional Fermi surface's area perpendicular to the magnetic field increases when moving from $B \parallel c$ to $B \parallel b$, so does the real-space cyclotron orbit, reducing the MR. Meanwhile, given the fixed temperature, the mean free path between two scattering events in the direction parallel to the a axes stays constant. Overall, the ratio l_e/r_c decreases.

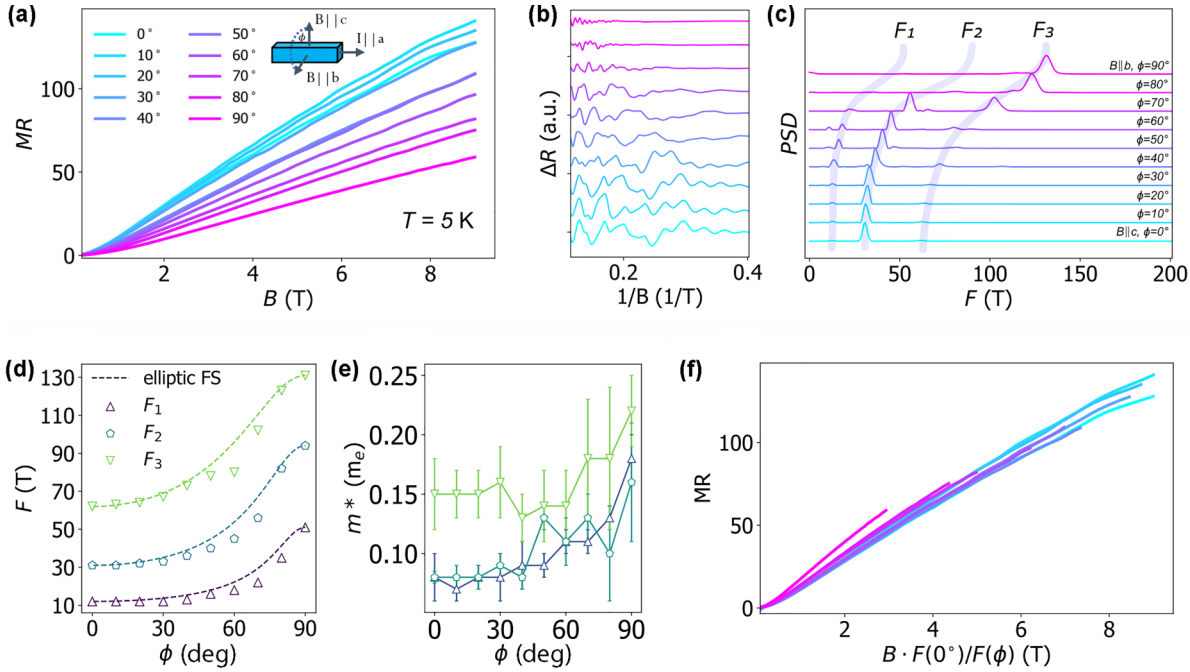

FIG. 2. Angle-dependent MR and FS shape. (a) Angle-dependent MR at $T = 5$ K vs field, from $B \parallel c$ ($\phi = 0°$) to $B \parallel b$ ($\phi = 90°$). (b) SdH oscillations isolated from the smooth background. (c) Oscillations' PSD at different angles. Three main oscillation frequencies are highlighted. (d) Oscillation frequencies and (e) effective masses vs angle. The oscillations' frequencies are fitted considering elliptic FSs [dashed lines in (d)]. (f) Angle-dependent MR at $T = 5$ K vs field times the inverse of normalized oscillations' frequency, which is proportional to the relative change of the cyclotron radius. The MR curves almost collapse on a single line, suggesting that its angle dependence mostly comes from the angle-dependent cyclotron orbit.

From the angle-dependent SdH we can measure the cyclotron radius $r_c(\phi)$ perpendicular to the transport direction and to the magnetic field, and compare it with the angle-dependent MR.

Because of the elliptic Fermi surface the cyclotron orbit is also elliptic, and the ratio between oscillation frequencies at different ϕ is equal to the ratio between the major and minor axis of the orbit. This is because, while rotating the magnetic field, only one of the radii changes, while the other stays constant,

$$\frac{F(\phi)}{F(0^\circ)} = \frac{A_{\mathrm{FS}}(\phi)}{A_{\mathrm{FS}}(0^\circ)} \approx \frac{\pi r_{c0} r_c(\phi)}{\pi r_{c0}^2} = \frac{r_c(\phi)}{r_{c0}}, \qquad (2)$$

where F is the SdH frequency, A_{FS} the FS area, r_{c0} is the minor axis of the ellipsoid sphere, and $r_c(\phi)$ is the major axis. In Fig. 2(f), the plot of the MR as a function of the magnetic field renormalized by the relative cyclotron radius [or relative oscillation frequency, Eq. (2)] causes the angle-dependent MR curves to almost collapse on a single line, similar to what is shown in the Kohler plot in Fig. 1(g).

Only the SdH frequencies F_2 of Fig. 2(c) are used in the renormalization. This is because up to $\phi = 60^\circ$ F_2 clearly dominates the PSD and the angle dependence is similar for all the observed frequencies. Also, the scattering rate is considered isotropic. The approximation of considering only one pocket with an isotropic scattering rate in the analysis of the MR could justify the deviation from a perfect collapse in Fig. 2(f). This result suggests that the cyclotron radius perpendicular to the transport direction is the main parameter regulating the angle-dependent MR. The collapse shown in Fig. 2(f) remains valid up to 300 K (Fig. S4 in the Supplemental Material [26]), meaning that it is independent of the specific scattering mechanism, which affects l_e but not r_c.

Commonly, the angle-dependent MR is associated with the angle-dependent effective mass or mobility [31,32], rather than the cyclotron radius. To test whether the notion of MR scaling with the effective mass is useful for the description of NbP, in Fig. 2(e) we extracted the angle-dependent effective mass from the temperature dependence of the SdH oscillations amplitude (Fig. S5 in the Supplemental Material [26]). The relative increase of the effective masses with angle is smaller than the relative increase of r_c with angle, and cannot describe the change in MR. Also, the extracted effective masses are subject to a larger uncertainty than the oscillation frequencies, making the latter an easier quantity to deal with.

The cyclotron radius of the NbP carriers' orbit is as small as 20 nm, for $B = 9$ T and parallel to the c axis, while the mean free path is around 7.7 μm at 4 K, which gives $l_e/r_c = 384$. In normal metals under the same conditions the situation is generally the opposite, namely, the mean free path is in the nanometer range, while the cyclotron radius can be several micrometers, justifying the tremendously lower values of MR, when compared to XMR materials such as NbP, despite being apparently regulated by similar mechanisms.

IV. CONCLUSION

In summary, the temperature dependence of the XMR of NbP can be understood in terms of temperature-dependent mobility, and the angle-dependent XMR relates to the

variation of the cyclotron orbit as the magnetic field is rotated. The ratio l_e/r_c, that is around 380 in our NbP sample at 4 K and 9 T, controls the magnitude of the XMR. This is not different from what happens in normal metals, where the MR is several orders of magnitude lower than that of XMR materials such as NbP. The difference lies on the fact that Dirac and Weyl semimetals are characterized by exceptionally long mean free paths and short cyclotron radii, i.e., very high mobilities and small Fermi surfaces, while the situation can be the opposite in normal metals.

The presence of multiple carriers of different species in an almost-compensated proportion is another crucial aspect required to explain the magnitude as well as the nonparabolic and nonsaturating MR, but a simplified model in which only the most mobile carriers' pocket is considered (a pocket of Weyl electrons in the NbP case) appears to be enough to explain the variation of MR with temperature and magnetic field direction.

ACKNOWLEDGMENTS

We wish to acknowledge the support of the Cleanroom Operations Team of the Binnng and Rohrer Nanotechnology Center (BRNC). F.B. and B.G. acknowledge the SNSF project HYDRONICS. under the Sinergia grant (No. 189924). L.R. and C.Z. acknowledge the SNSF Ambizione programme. A.M. acknowledges funding support from the European Union's Horizon 2020 research and innovation programme under the Marie Sklodowska-Curie Grant Agreement No. 898113 (InNaTo). C.Z., H.S., A.M., V.S, C.F., and B.G. acknowledge the European Union's FET open project No. 829044 (SCHINES).

[1] N. Kumar, Y. Sun, N. Xu, K. Manna, M. Yao, V. Süss, I. Leermakers, O. Young, T. Förster, M. Schmidt, H. Borrmann, B. Yan, U. Zeitler, M. Shi, C. Felser, and C. Shekhar, Extremely high magnetoresistance and conductivity in the type-II Weyl semimetals WP_2 and MoP_2, Nat. Commun. **8**, 1642 (2017).

[2] C. Shekhar, A. K. Nayak, Y. Sun, M. Schmidt, M. Nicklas, I. Leermakers, U. Zeitler, Y. Skourski, J. Wosnitza, Z. Liu, Y. Chen, W. Schnelle, H. Borrmann, Y. Grin, C. Felser, and B. Yan, Extremely large magnetoresistance and ultrahigh mobility in the topological Weyl semimetal candidate NbP, Nat. Phys. **11**, 645 (2015).

[3] T. Liang, Q. Gibson, M. N. Ali, M. Liu, R. J. Cava, and N. P. Ong, Ultrahigh mobility and giant magnetoresistance in the Dirac semimetal Cd_3As_2, Nat. Mater. **14**, 280 (2015).

[4] C. Zhang, C. Guo, H. Lu, X. Zhang, Z. Yuan, Z. Lin, J. Wang, and S. Jia, Large magnetoresistance over an extended temperature regime in monophosphides of tantalum and niobium, Phys. Rev. B **92**, 041203(R) (2015).

[5] M. N. Baibich, J. M. Broto, A. Fert, F. Nguyen Van Dau, F. Petroff, P. Etienne, G. Creuzet, A. Friederich, and J. Chazelas, Giant magnetoresistance of (001)Fe/(001)Cr magnetic superlattices, Phys. Rev. Lett. **61**, 2472 (1988).

[6] A. P. Ramirez, Colossal magnetoresistance, J. Phys.: Condens. Matter **9**, 8171 (1997).

[7] A. Toniato, B. Gotsmann, E. Lind, and C. B. Zota, Weyl semi-metal-based high-frequency amplifiers, in *2019 IEEE International Electron Devices Meeting (IEDM)* (IEEE, New York, 2019), pp. 9.4.1–9.4.4.

[8] R. Niu and W. K. Zhu, Materials and possible mechanisms of extremely large magnetoresistance: A review, J. Phys.: Condens. Matter **34**, 113001 (2022).

[9] M. Matin, R. Mondal, N. Barman, A. Thamizhavel, and S. K. Dhar, Extremely large magnetoresistance induced by Zeeman effect-driven electron-hole compensation and topological protection in $MoSi_2$, Phys. Rev. B **97**, 205130 (2018).

[10] F. Fallah Tafti, Q. Gibson, S. Kushwaha, J. W. Krizan, N. Haldolaarachchige, and R. J. Cava, Temperaturefield phase diagram of extreme magnetoresistance, Proc. Natl. Acad. Sci. USA **113**, E3475 (2016).

[11] J. Xu, N. J. Ghimire, J. S. Jiang, Z. L. Xiao, A. S. Botana, Y. L. Wang, Y. Hao, J. E. Pearson, and W. K. Kwok, Origin of the extremely large magnetoresistance in the semimetal YSb, Phys. Rev. B **96**, 075159 (2017).

[12] S. Singh, V. Süß, M. Schmidt, C. Felser, and C. Shekhar, Strong correlation between mobility and magnetoresistance in Weyl and Dirac semimetals, J. Phys. Mater. **3**, 024003 (2020).

[13] N. H. Jo, Y. Wu, L.-L. Wang, P. P. Orth, S. S. Downing, S. Manni, D. Mou, D. D. Johnson, A. Kaminski, S. L. Bud'ko, and P. C. Canfield, Extremely large magnetoresistance and Kohler's rule in $PdSn_4$: A complete study of thermodynamic, transport, and band-structure properties, Phys. Rev. B **96**, 165145 (2017).

[14] Y.-Y. Lv, X. Li, J. Zhang, B. Pang, S.-S. Chen, L. Cao, B.-B. Zhang, D. Lin, Y. B. Chen, S.-H. Yao, J. Zhou, S.-T. Zhang, M.-H. Lu, M. Tian, and Y.-F. Chen, Mobility-controlled extremely large magnetoresistance in perfect electron-hole compensated α-WP_2 crystals, Phys. Rev. B **97**, 245151 (2018).

[15] P. Kumar, Sudesh, and S. Patnaik, Origin of exceptional magneto-resistance in Weyl semimetal $TaSb_2$, J. Phys. Commun. **3**, 115007 (2019).

[16] Y. L. Wang, L. R. Thoutam, Z. L. Xiao, J. Hu, S. Das, Z. Q. Mao, J. Wei, R. Divan, A. Luican-Mayer, G. W. Crabtree, and W. K. Kwok, Origin of the turn-on temperature behavior in WTe_2, Phys. Rev. B **92**, 180402(R) (2015).

[17] A. B. Pippard, *Magnetoresistance in Metals* (Cambridge University Press, Cambridge, UK, 1989).

[18] K. Noto and T. Tsuzuku, A simple two-band theory of galvanomagnetic effects in graphite in relation to the magnetic field azimuth, Jpn. J. Appl. Phys. **14**, 46 (1975).

[19] M. Kohler, Zur magnetischen Widerstandsänderung reiner Metalle, Ann. Phys. **424**, 211 (1938).

[20] A. A. Abrikosov, *Fundamentals of the Theory of Metals* (Dover, New York, 1988).

[21] N. Luo and G. Miley, Kohler's rule and relaxation rates in high-T_c superconductors, Physica C: Supercond. **371**, 259 (2002).

[22] J. Xu, F. Han, T.-T. Wang, L. R. Thoutam, S. E. Pate, M. Li, X. Zhang, Y.-L. Wang, R. Fotovat, U. Welp, X. Zhou, W.-K. Kwok, D. Y. Chung, M. G. Kanatzidis, and Z.-L. Xiao, Extended

Kohler's rule of magnetoresistance, Phys. Rev. X **11**, 041029 (2021).

[23] J. Klotz, S.-C. Wu, C. Shekhar, Y. Sun, M. Schmidt, M. Nicklas, M. Baenitz, M. Uhlarz, J. Wosnitza, C. Felser, and B. Yan, Quantum oscillations and the Fermi-surface topology of the Weyl semimetal NbP, Phys. Rev. B **93**, 121105(R) (2016).

[24] P. J. Moll, Focused ion beam microstructuring of quantum matter, Annu. Rev. Condens. Matter Phys. **9**, 147 (2018).

[25] M. D. Bachmann, N. Nair, F. Flicker, R. Ilan, T. Meng, N. J. Ghimire, E. D. Bauer, F. Ronning, J. G. Analytis, and P. J. W. Moll, Inducing superconductivity in Weyl semimetal microstructures by selective ion sputtering, Sci. Adv. **3**, e1602983 (2017).

[26] See Supplemental Material at http://link.aps.org/supplemental/10.1103/PhysRevB.109.045148 for additional data of Hall effect, angle-dependent MR, angle-dependent SdH, and results repeated on a second sample.

[27] B. F. Gao, P. Gehring, M. Burghard, and K. Kern, Gate-controlled linear magnetoresistance in thin Bi_2Se_3 sheets, Appl. Phys. Lett. **100**, 212402 (2012).

[28] Z. Hou, B. Yang, Y. Wang, B. Ding, X. Zhang, Y. Yao, E. Liu, X. Xi, G. Wu, Z. Zeng, Z. Liu, and W. Wang, Large and anisotropic linear magnetoresistance in single crystals of black phosphorus arising From mobility fluctuations, Sci. Rep. **6**, 23807 (2016).

[29] P. Kapitza, The study of the specific resistance of bismuth crystals and its change in strong magnetic fields and some allied problems, Proc. R. Soc. London, Ser. A **119**, 358 (1928).

[30] P. M. C. Rourke and S. R. Julian, Numerical extraction of de Haas–van Alphen frequencies from calculated band energies, Comput. Phys. Commun. **183**, 324 (2012).

[31] L. R. Thoutam, Y. L. Wang, Z. L. Xiao, S. Das, A. Luican-Mayer, R. Divan, G. W. Crabtree, and W. K. Kwok, Temperature dependent three-dimensional anisotropy of the magnetoresistance in WTe_2, Phys. Rev. Lett. **115**, 046602 (2015).

[32] O. Pavlosiuk, P. W. Swatek, J.-P. Wang, P. Wiśniewski, and D. Kaczorowski, Giant magnetoresistance, Fermi-surface topology, Shoenberg effect, and vanishing quantum oscillations in type-II Dirac semimetal candidates $MoSi_2$ and WSi_2, Phys. Rev. B **105**, 075141 (2022).